Polarization Mode Dispersion Compensation at 10, 20, and 40 Gb/s with Various Optical Equalizers

Reinhold Noé, David Sandel, M. Yoshida-Dierolf, Stephan Hinz, V. Mirvoda, A. Schöpflin, C. Glingener, E. Gottwald, C. Scheerer, G. Fischer, Thomas Weyrauch, and Wolfgang Haase

Abstract— **Polarization mode dispersion (PMD), especially in "old" fibers, is considered harmful for installation and upgrading of trunk lines. An optical PMD equalizer should have several or many differential group delay (DGD) sections with polarization transformers in between which can endlessly transform any input polarization into a principal state of the following DGD section. The sections must practically have fixed DGD's unless there is only one section. The small-signal baseband transfer function for PMD, higher order PMD, and the necessary number of sections as well as their control by the output signals of an electrical filter bank in the receiver are also discussed in this context. Several PMD equalizers have been realized and successfully tested in transmission systems with bit rates of 10, 20, and 40 Gb/s. The systems operated stably with well-opened eye diagrams for DGD's ranging between 0 and 1.7 bit durations. Best performance is obtained from a distributed PMD equalizer with one piece of polarization-maintaining fiber twisted by 64 stepper motors. The principle can also be realized in LiNbO₃.**

Index Terms— **Compensation, equalizers, optical fiber communication, optical polarization mode dispersion, polarization, polarization mode dispersion.**

I. INTRODUCTION

POLARIZATION mode dispersion (PMD) [1] relates to the random anisotropy of long lengths of single-mode fiber, caused by noncircular cores and transversal stress due to bending and cabling. There exist *principal states-of-polarization* (PSP's) which have the maximum possible group delay difference or *differential group delay* (DGD). If a PSP is excited at the fiber input impulses will propagate undistorted, and the signal will stay completely polarized because the output polarization remains constant to first order as a function of optical frequency. If the signal polarization is a mixture between the PSP's impulse broadening occurs in the time domain, and the signal becomes depolarized in the frequency domain.

After fiber attenuation and chromatic dispersion, polarization mode dispersion is the next obstacle in the development of

high-capacity, long-haul optical communication systems [2]. PMD is intricate to tackle because it may vary as a function of time or fiber temperature. In the optical domain, previous work to compensate PMD has focused on selecting a PSP of the transmission line by input polarization control [3] or implementing a compensator consisting of a small number of DGD sections, separated by polarization transformers [4]–[6]. In the former case the control speed is limited by the propagation delay and complicated by the required back channel. In the latter case which this paper is about speed and insertion loss of polarization transformers, and possibly a variation of a DGD section are key issues. In the electrical part of an optical receiver, PMD can be equalized by transversal filters or quantized feedback [7]. Since the photocurrent is proportional to the squared field vector magnitude not all PMD distortions can be undone electronically, and we concentrate therefore on the optical solutions.

We explain the optical and electrical requirements for an automatic PMD compensation system (Section II), present various optical equalizers (Section III), describe transmission experiments with automatic PMD compensation (Section IV), and finally compare the relative merits of the different components and systems (Section V).

II. DESIGN CONSIDERATIONS FOR A PMD COMPENSATION SYSTEM

A. Structure and Function of an Optical Equalizer

In order to be able to compensate PMD a suitable equalizer structure must be found. In this subsection, we will derive the necessary properties of polarization transformers and differential group delay sections. Transmission span and equalizer are assumed to consist of lossless optical retarders, and isotropic propagation delays are neglected. The retarders can be described by unitary 2×2 Jones matrices or by reduced Mueller matrices in which the first row and column has been eliminated, i.e., orthogonal 3×3 matrices. The latter rotation matrices turn input normalized Stokes vectors $[S_1 \ S_2 \ S_3]^T$ on the Poincaré sphere surface into output normalized Stokes vectors.

The most general retarder is an endless elliptical retarder (ER). It is described by (1) and (2) shown at the bottom of the next page in Jones and Mueller formulation, respectively. Relative strengths of $0°$, $45°$ and circular birefringence are given by V_1, V_2, and V_3, respectively. These as well as the retardation $\varphi = -\infty \ldots \infty$ can vary endlessly. EM (Jones or

normalized Stokes vector) is one of the eigenmodes, the faster one for positive φ. Its polarization ellipse is characterized by azimuth angle ϑ and ellipticity angle ϵ. Angles $2\vartheta = -\infty \ldots \infty$ and $2\varepsilon = -\pi/2 \ldots \pi/2$ are spherical coordinates on the Poincaré sphere and allow for endless variations of the eigenmodes. Linear birefringence (core ellipticity, bending, transverse stress) and fiber twist (optical activity) may coexist and may vary along a singlemode fiber. A fiber should or even must therefore be represented by an ER at a given optical frequency.

Both Jones and Mueller matrices of optical components can be multiplied in reversed order of light propagation to describe their concatenation. This means expressions (3)–(11) are valid for Jones matrices (1) and for (reduced) Mueller matrices (2). We use the nomenclature

(endless) phase shifter ($2\vartheta = 0, 2\varepsilon = 0$):
$$\text{PS}(\varphi = -\infty \ldots \infty),$$
(finite) mode converter ($2\vartheta = \pi/2, 2\varepsilon = 0$):
$$\text{MC}(\varphi = 0 \ldots \pi),$$
(endless) Soleil–Babinet compensator ($2\varepsilon = 0$):
$$\text{SBC}(\varphi = 0 \ldots \pi, 2\vartheta = -\infty \ldots \infty),$$
(endless) Soleil–Babinet analogon ($2\vartheta = \pi/2$):
$$\text{SBA}(\varphi = 0 \ldots \pi, 2\varepsilon = -\infty \ldots \infty) \tag{3}$$

to define some special cases of an ER. We call the last example a Soleil–Babinet analogon because it is related to the familiar Soleil–Babinet compensator, a rotatable waveplate of adjustable retardation, by cyclical shifts of rows and columns of the reduced Mueller matrix. A rotating SBC ($2\vartheta = \Omega t$) converts circular input polarization partly or fully into its orthogonal including a frequency shift by Ω. A "rotating" SBA ($2\varepsilon = \Omega t$) does the same thing to an x-polarized input signal. An SBA can endlessly transform x polarization at its input into any output polarization or vice versa. An SBA can be replaced by a phase shifter, a mode converter, and another phase shifter of opposite retardation

$$\text{SBA}(\varphi, 2\varepsilon) = \text{PS}(2\varepsilon)\text{MC}(\varphi)\text{PS}(-2\varepsilon). \tag{4}$$

An ER is equivalent of a sequence of a quarterwave plate, a halfwave plate, and another quarterwave plate, each of them

Fig. 1. Transmission span (TS) with elliptical retarders (ER) and DGD sections. Suitable equalizer (EQ) with Soleil–Babinet analogons (SBA; see text) and DGD sections, each of which may be accompanied by arbitrary differential phase shifts.

endlessly rotatable [8]. We have verified that an ER may also be realized by an endlessly rotatable halfwave plate and an SBC. Alternatively, an ER can be replaced by a phase shifter, a mode converter, and another phase shifter [9]. In a lengthy proof we have found that the mode converter needs only a finite retardation in the range $0 \ldots \pi$. This means the ER can also be substituted by an SBA, preceded or followed by one PS:

$$\begin{aligned} \text{ER} &= \text{PS}(\varphi_3)\text{MC}(\varphi_2)\text{PS}(\varphi_1) \\ &= \text{PS}(\varphi_3 + \varphi_1)\text{SBA}(\varphi_2, -\varphi_1) \\ &= \text{SBA}(\varphi_2, \varphi_3)\text{PS}(\varphi_1 + \varphi_3). \end{aligned} \tag{5}$$

Comparison of the last two expressions shows that a phase shifter may be "pushed" from left to right through a SBA if the SBA orientation angle is increased by the transferred phase shift. At an angular optical frequency ω we represent a fiber section having a differential group delay τ by a phase shifter $\text{PS}(\omega\tau)$. Its eigenmodes and principal states-of-polarization (PSP) coincide. The whole transmission span TS may consist of an infinite sequence of alternating ER's and DGD sections. In practice, we limit ourselves to N DGD sections and $N+1$ ER's which are passed by the light signal in ascending order of index i (Fig. 1)

$$\begin{aligned} \text{TS} &= \prod_{i=N}^{1} (\text{ER}_i\text{PS}(\omega\tau_i)) \, \text{ER}_0 \\ &= \prod_{i=N}^{1} (\text{SBA}(\varphi_{2i}, \varphi_{3i})\text{PS}(\varphi_{1i} + \varphi_{3i} + \omega\tau_i)) \, \text{ER}_0. \end{aligned} \tag{6}$$

$$\text{ER} = \begin{bmatrix} \cos\varphi/2 + jV_1\sin\varphi/2 & j(V_2 + jV_3)\sin\varphi/2 \\ j(V_2 - jV_3)\sin\varphi/2 & \cos\varphi/2 - jV_1\sin\varphi/2 \end{bmatrix}$$

$$\text{EM} = \frac{1}{\sqrt{2(1+V_1)}} \begin{bmatrix} 1 + V_1 \\ V_2 - jV_3 \end{bmatrix} \qquad (V_1^2 + V_2^2 + V_3^2 = 1) \tag{1}$$

or

$$\text{ER} = \begin{bmatrix} V_1^2 + (V_2^2 + V_3^2)\cos\varphi & V_1V_2(1 - \cos\varphi) - V_3\sin\varphi & V_1V_3(1 - \cos\varphi) + V_2\sin\varphi \\ V_1V_2(1 - \cos\varphi) + V_3\sin\varphi & V_2^2 + (V_1^2 + V_3^2)\cos\varphi & V_2V_3(1 - \cos\varphi) - V_1\sin\varphi \\ V_1V_3(1 - \cos\varphi) - V_2\sin\varphi & V_2V_3(1 - \cos\varphi) + V_1\sin\varphi & V_3^2(V_1^2 + V_2^2)\cos\varphi \end{bmatrix}$$

$$\text{EM} = \begin{bmatrix} V_1 \\ V_2 \\ V_3 \end{bmatrix} = \begin{bmatrix} \cos 2\vartheta\cos 2\varepsilon \\ \sin 2\vartheta\cos 2\varepsilon \\ \sin 2\varepsilon \end{bmatrix} \qquad (V_1^2 + V_2^2 + V_3^2 = 1) \tag{2}$$

The product symbols with a stop index 1 that is lower than the start index N have to be written from left to right in descending order of index i. Adjacent phase shifts or shifters may be interchanged. All frequency-independent phase shifts in the second expression can therefore be transferred to the right through preceding SBA's according to (5)

$$\text{TS} = \prod_{i=N}^{1} \left(\text{SBA}\left(\varphi_{2,i}, \varphi_{3i} + \sum_{k=i+1}^{N} (\varphi_{1k} + \varphi_{3k}) \right) \text{PS}(\omega\tau_i) \right)$$
$$\cdot \text{PS}\left(\sum_{i=1}^{N} (\varphi_{1i} + \varphi_{3i}) \right) \text{ER}_0. \tag{7}$$

The PMD equalizer has to mirror the PMD profile of the transmission span. In a particular implementation EQ' it may consist of the same sequence of SBA's and DGD sections as the TS, but with reversed order. The signs of SBA and PS retardations are inverted which can also be accomplished by orthogonal orientations.

$$\text{EQ}' = \prod_{i=1}^{N} \left(\text{PS}(-\omega\tau_i) \right.$$
$$\left. \cdot \text{SBA}\left(-\varphi_{2,i}\varphi_{3i} + \sum_{k=i+1}^{N} (\varphi_{1k} + \varphi_{3k}) \right) \right). \tag{8}$$

The phase delay $-\omega\tau_i$ of a DGD section may be of the order of many, many 2π. It is therefore practically impossible to avoid frequency-independent, possibly endless offset retardations $\varphi_{4i} = -\infty \ldots \infty$ in each DGD section. However, these can be taken care of by moving them through subsequent SBA's, i.e., to the left, according to (5). In this generalized implementation with additional degrees of freedom the equalizer (EQ) is described by

$$\text{EQ} = \prod_{i=1}^{N} \left(\text{PS}(-\omega\tau_i + \varphi_{4i}) \right.$$
$$\left. \cdot \text{SBA}\left(-\varphi_{2,i}, \varphi_{3i} + \sum_{k=i+1}^{N} (\varphi_{4k} + \varphi_{1k} + \varphi_{3k}) \right) \right). \tag{9}$$

As desired, the concatenation of TS and EQ (or EQ') results in a frequency-independent ER that does not exhibit any PMD

$$\text{EQ} \cdot \text{TS} = \text{PS}\left(\sum_{i=1}^{N} (\varphi_{4i} + \varphi_{1i} + \varphi_{3i}) \right) \text{ER}_0 = \text{ER} \tag{10}$$

Although suggested by (9), the polarization transformers in the EQ need not necessarily be SBA's. We may substitute $\varphi_{4i} = \varphi'_{4i} + \varphi''_{4i}$ and consider $\text{PS}(\varphi'_{4i})$ to be part of a DGD section $\text{PS}(-\omega\tau_i + \varphi'_{4i})$ while $\text{PS}(\varphi''_{4i})$ belongs to the preceding polarization transformer. The ith polarization transformer, now described by

$$\text{PS}(\varphi''_{4,i}) \, \text{SBA}\left(-\varphi_{2,i}, \varphi_{3i} \right.$$
$$\left. + \sum_{k=i+1}^{N} (\varphi'_{4k} + \varphi''_{4k} + \varphi_{1k} + \varphi_{3k}) \right) \tag{11}$$
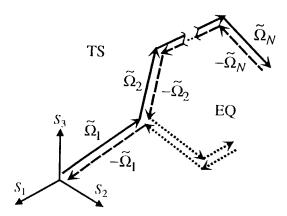

Fig. 2. PMD profile of transmission span (solid) and perfect equalizer (dashed, dotted) in the three-dimensional normalized Stokes space.

is an ER (5) if its three variables, one for the PS and two for the SBA, are independent. However, to minimize efforts the designer should let φ''_{4i} depend on the two SBA parameters at will, thereby retaining only two independent variables. Such a polarization transformer may be easier to realize than a true SBA, as will be seen in Section III. Like the SBA it has the property of being able to *endlessly transform any input polarization into a PSP of the following DGD section.* It is indeed a PSP we need to consider here, not just an eigenmode. To see this we place another retarder and its inverse between $\text{PS}(\varphi''_{4i})$ and $\text{PS}(-\omega\tau_i + \varphi'_{4i})$. One of them is considered to belong to $\text{PS}(-\omega\tau_i + \varphi'_{4i})$ where it transforms PSP's (but modifies EM's in a different way), while the other is part of the polarization transformer.

PMD may be illustrated graphically as mentioned in [10], [11]. The PMD profile of concatenated retarders is a sequence of input-referred PMD vectors $\tilde{\Omega}_i$.

$$\tilde{\Omega}_i = R_{<i}^T \Omega_i, \quad \tilde{\Omega}_{\text{total}} = \sum \tilde{\Omega}_i, \quad \tau_{\text{total}} = 2|\tilde{\Omega}_{\text{total}}|. \tag{12}$$

Matrix $R_{<i}$ is a 3×3 matrix (2) representing the concatenated retarders preceding the retarder with PMD vector Ω_i. Ω_i is the normalized Stokes vector of a PSP, multiplied by half the DGD. In the transmission span of Fig. 1, $\Omega_i = [1\ 0\ 0]^T \tau_i/2$ and the direction change between PMD vectors $\tilde{\Omega}_i$ and $\tilde{\Omega}_{i+1}$ is mediated by the rotation matrix ER_i (2). The sum is the PMD vector $\tilde{\Omega}_{\text{total}}$. It can be shown that $\tilde{\Omega}_{\text{total}}$ represents PSP's and DGD τ_{total} of the concatenation by its direction and twice its length, respectively, thereby justifying the use of PMD vectors. Fig. 2 shows the PMD profile of the concatenation of TS and a perfect EQ fulfilling (10). All PMD vectors are cancelled by opposed adjacent ones because PMD is compensated not just to 1st order (which merely requires the vector sum and thereby τ_{total} to vanish) but completely (assuming all existing frequency dependence has been covered by vectors Ω_i). As exemplified by the dotted arrows, an excess of total DGD of the EQ over that of the TS is not of concern if some adjacent compensator sections are made to cancel each other. Less perfect PMD vector cancelling normally indicates a PMD penalty. Provided the signal happens to coincide with a PSP it may be transmitted without distortion if merely first-order PMD persists after the EQ.
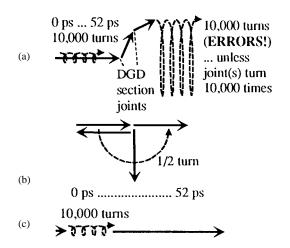
Fig. 3. (a) Variable DGD section equalizer has speed problem. (b) Transmission span most easily changes PMD vector orientations, and so does a fixed DGD section equalizer. (c) Pure DGD vector lengthening is unlikely to happen in a transmission span.

An important practical question is whether a PMD compensator should have fixed or variable DGD sections, and there is a straight answer to it. It may be calculated that fixed differential group delays can cause detrimental side maxima of compensator performance. An immediate argument in favor of a variable DGD compensator is therefore that side maxima vanish. This is useful and important for one-section equalizers which, however, leave second- and higher order PMD uncompensated.

The situation turns out to be different for equalizers with more than one section: What happens if the DGD of the first section (denominated as $-\tilde{\Omega}_N$ in Fig. 2) of a two- or even multisection EQ with *variable* DGD's has to slide from 0 to 52 ps? The latter value corresponds to roughly 10 000 periods of a 1550 nm lightwave. The DGD increase corresponds to a lengthening of this vector by a screw motion with a pitch of one lightwave period of DGD change per turn. If the subsequent DGD vectors (denominated as $-\tilde{\Omega}_{N-1} \ldots -\tilde{\Omega}_1$) are connected to it by fixed joints ($=$ SBA's with frozen parameters) the PMD profile will change shape during each screw turn, which is highly detrimental [Fig. 3(a)]. If the joints are of rotary type ($=$ SBA's with variable orientations) the PMD profile may stay the same because all subsequent DGD vectors may revolve in place 10 000 times like axes connected by rotary joints. If the first section is followed by a ball-and-socket joint ($=$ ER with three degrees-of-freedom) only this latter has to turn 10 000 times. The issue can also be understood from (12) where $\tilde{\Omega}_i$ depends on $R_{<i}$. Now, if we consider that each of the 10 000 turns of the joint(s) (SBA's or ER) may need between 10 and 100 optimization steps it becomes clear that variable DGD sections are unpractical due to the huge required number of SBA (or ER) adjustment steps, except for the last section which has no subsequent SBA. For comparison, consider two *fixed* 26 ps DGD sections in the compensator. Changing the SBA (or ER) in between these two by a retardation of just π will flip the DGD profile open like

Fig. 4. Small-signal transfer model of a PMD medium.

a pocketknife from 0 ps to a total DGD of 52 ps [Fig. 3(b)], and this is about 10 000 times faster than the previous case.

But could a fixed DGD equalizer follow if a TS chose to vary its PMD profile by lengthening a DGD vector? Here we explain why substantial DGD vector length changes are unlikely to happen: Consider a TS with two *fixed* 26 ps DGD sections. As already explained, a DGD change of 52 ps requires just a retardation change of π for the SBA (or ER) in between them [Fig. 3(b)]. In contrast, a pure 52 ps DGD *growth* (PMD vector lengthening) requires a much higher retardation change of $10{,}000 \cdot 2\pi$ and therefore occurs with a negligibly small probability [Fig. 3(c)].

As a consequence, *an equalizer with fixed DGD sections is a natural PMD compensator for a fiber transmission span* whereas more than one variable DGD section of an equalizer can practically not be used as such. Nevertheless, a single-section, variable DGD equalizer is able to compensate first-order PMD.

B. Small-Signal Baseband Transfer Function

Clearly, the impact of PMD caused by transmission span or equalizer can easily be calculated numerically. Eye closure is a usual result of this treatment. We believe it is instructive to derive an analytical small-signal model of a system under the influence of PMD.

In Fig. 4, a simple optical transmission system with a transmitter, a PMD medium, and a receiver is shown. The optical power is sinusoidally modulated around its mean value with a small modulation depth, $|a| \ll 1$. At the receiver output the modulation signal appears with changed amplitude and a phase shift. This can be expressed by a complex baseband transfer function $H(\omega)$. Suitably normalized, the simple result

$$H(\omega) = (1/2)e_{\text{in}}^+(J^+(\omega_0)J(\omega_0 + \omega)J^+(\omega_0 - \omega)J(\omega_0))e_{\text{in}} \tag{13}$$

is obtained, where ω is the modulation frequency, ω_0 the optical carrier frequency, e_{in} the Jones vector of the input polarization, and J the Jones matrix of the medium. Consider a medium which exhibits only first-order PMD, e.g., a single section of DGD τ preceded and followed by arbitrary frequency-independent polarization transformers. In this simple case we can express $H(\omega)$ as

$$H(\omega) = \cos(\omega\tau/2) + j\tilde{\Omega}_n^T S_{\text{in}} \sin(\omega\tau/2) \tag{14}$$

where $\tilde{\Omega}_n = \tilde{\Omega}/|\tilde{\Omega}| = 2\tilde{\Omega}/\tau$ is the normalized Stokes vector of the fast PSP [see (12)]. If we set the input polarization (normalized Stokes vector S_{in}) to be equal to one of the PSP's the resulting transfer function is $H(\omega) = e^{\pm j\omega\tau/2}$ which identifies τ to be the DGD. This means the original derivation [1] of PSP's and DGD could be replaced by the small-signal transfer function approach. PMD vector $\tilde{\Omega}$ can be derived from
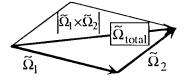
Fig. 5. Geometrical interpretation of second-order PMD effect.

the elements of the Jones matrix $\boldsymbol{J}$ as

$$\tilde{\Omega} = \begin{bmatrix} \mathrm{Im}(u_1^* \dot{u}_1 + u_2 \dot{u}_2^*) \\ \mathrm{Re}(j(u_2 \dot{u}_1^* - u_1^* \dot{u}_2)) \\ \mathrm{Im}(j(u_2 \dot{u}_1^* - u_1^* \dot{u}_2)) \end{bmatrix} \quad \text{with}$$

$$\boldsymbol{J} = \begin{bmatrix} u_1 & u_2 \\ -u_2^* & u_1^* \end{bmatrix}, \quad |u_1|^2 + |u_2|^2 = 1 \tag{15}$$

where the dot denotes a differentiation with respect to the optical carrier frequency ω_0. Equation (14) also confirms that the 101010 sequences disappear if the input polarization is in between the two PSP's ($\tilde{\Omega}_n^T \boldsymbol{S}_{\mathrm{in}} = 0$)) and the DGD approaches one bit duration. Of course, we can approximate $H(\omega) \approx 1 + j\omega \tilde{\Omega}^T \boldsymbol{S}_{\mathrm{in}}$ for $|\omega \tau/2| \ll 1$.

Next consider two DGD sections (indexes 1, 2), preceded, separated, and followed by polarization transformers. In terms of Stokes vectors the resulting baseband transfer function is

$$\begin{aligned} H(\omega) = {} & \cos(\omega\tau_1/2)\cos(\omega\tau_2/2) \\ & - \sin(\omega\tau_1/2)\sin(\omega\tau_2/2)\tilde{\Omega}_{1n}^T \tilde{\Omega}_{2n} \\ & + j(\sin(\omega\tau_1/2)\cos(\omega\tau_2/2)\tilde{\Omega}_{1n}^T \\ & + \sin(\omega\tau_2/2)\cos(\omega\tau_1/2)\tilde{\Omega}_{2n}^T)\boldsymbol{S}_{\mathrm{in}}. \end{aligned} \tag{16}$$

Equation (14) is an approximation of (16) if we use $\tilde{\Omega}_{\mathrm{total}}$ calculated according to (12). Assume now the input polarization is a PSP, $\boldsymbol{S}_{\mathrm{in}} = \pm\tilde{\Omega}_{n,\mathrm{total}}$. In this case the magnitude of $H(\omega)$ is maximized and may be approximated by

$$|H(\omega)|_{\max}^2 \approx 1 - (\omega^2 |\tilde{\Omega}_1 \times \tilde{\Omega}_2|)^2. \tag{17}$$

The squared magnitude depends on the outer product between the PMD vectors of the two DGD sections, i.e., the area defined by their PMD profile, see Fig. 5. Note that vectors $\tilde{\Omega}_2$ and $\tilde{\Omega}_{\mathrm{total}}$ gyrate about $\tilde{\Omega}_1$ if we tune the optical frequency.

This model can only be useful if its parameters can be fitted to approximate any given PMD device, and this is possible. The PMD vectors can be found from the results of a few optoelectrical measurements. The gradient of a quantity in the normalized Stokes space can be obtained from at least four measurements with different input states-of-polarization that inscribe a body of nonzero volume inside the Poincaré sphere. Four rather than three measurements are necessary because the isotropic group delay of the fiber must also be determined. Particularly well suited configurations are a regular tetrahedron or a regular hexahedron. The latter simply means that horizontal/vertical (measurements $N_1^{(\pm)}$), $\pm45°$ linear ($M_2^{(\pm)}$), and right/left circular polarizations ($M_3^{(\pm)}$) have to be applied sequentially. The gradient of quantity M is then

$$\mathrm{grad}\, M = \sum_{i=1}^{3} \boldsymbol{s}_i \frac{\partial M}{\partial S_i} = \sum_{i=1}^{3} \boldsymbol{s}_i \frac{M_i^{(+)} - M_i^{(-)}}{2} \tag{18}$$

with $\boldsymbol{s}_i$ being normalized unit Stokes vectors. Measurable vectors

$$\boldsymbol{u} = \mathrm{grad}\, \frac{\partial\, \mathrm{Im}(H)}{\partial\omega} = \tilde{\Omega}_{\mathrm{total}} = \tilde{\Omega}_1 + \tilde{\Omega}_2$$

$$\boldsymbol{v} = \frac{1}{2}\, \mathrm{grad}\, \frac{\partial^2\, \mathrm{Im}(H)}{\partial\omega_0 \partial\omega} = \tilde{\Omega}_2 \times \tilde{\Omega}_1$$

$$\boldsymbol{w} = -\frac{1}{4}\, \mathrm{grad}\, \frac{\partial^2\, \mathrm{Im}(H)}{\partial\omega_0^2 \partial\omega} = \tilde{\Omega}_1 \times \boldsymbol{v} \tag{19}$$

are thus defined. Vector $\boldsymbol{u}$ is obtained as the gradient of the negative group delay from electrical network analysis applied in Fig. 4. Vectors $\boldsymbol{v}$ and $\boldsymbol{w}$ need additional differentiations with respect to the optical frequency ω_0 which requires measurement at three different optical frequencies. The correctness of the expressions on the right side can be verified by inserting three ER's separated by two DGD sections into (13). The PMD vectors are found as

$$\tilde{\Omega}_1 = \frac{1}{|\boldsymbol{v}|^2}(\boldsymbol{v} \times \boldsymbol{w}) = \frac{\boldsymbol{u}\boldsymbol{u}^T}{|\boldsymbol{u}|^2 |\boldsymbol{v}|^2}(\boldsymbol{v} \times \boldsymbol{w}) - \frac{|\boldsymbol{v}|^2}{|\boldsymbol{u} \times \boldsymbol{v}^2|}(\boldsymbol{u} \times \boldsymbol{v})$$

$$\tilde{\Omega}_2 = \boldsymbol{u} - \tilde{\Omega}_1. \tag{20}$$

While the first expression for $\tilde{\Omega}_1$ is simpler the second may provide a better immunity against measurement errors. A polarimeter at the fiber output is not, but tunable optical source, polarization transformer, and electrical network analyzer or impulse response measurement are needed. Any PMD medium can be characterized by (20), or to first order by $\boldsymbol{u}$ alone. Similar relations are expected to exist for approximation of PMD media by more than two DGD sections.

Compare this to a definition of higher order PMD by a Taylor series expansion of the PMD vector after [12]

$$\Omega(\omega_0+\omega) = \underbrace{\Omega(\omega_0)}_{\text{1st}} + \underbrace{\dot{\Omega}(\omega_0)}_{\text{2nd}}\omega + \underbrace{(1/2!)\ddot{\Omega}(\omega_0)}_{\text{third order}}\omega^2 + \cdots. \tag{21}$$

The first term Ω is just our $\boldsymbol{u}$. Two components of $\dot{\Omega}$ are proportional to $\boldsymbol{v}$. Applied to the two-section model Fig. 5 these define the speed at and the direction in which $\tilde{\Omega}_{\mathrm{total}}$ gyrates about $\tilde{\Omega}_1$ if we tune the optical frequency ω_0. For a one- or two-section model the component of $\dot{\Omega}$ in direction of Ω may be assumed to be related to the DGD in a similar ratio as the chromatic dispersion is related to the total group delay (-5 ns/m) of a fiber. This means it is negligibly small compared to the two other components of $\dot{\Omega}$. The radius $|\tilde{\Omega}_2 \times \tilde{\Omega}_1|/|\tilde{\Omega}_1|$ of the gyration is obtained from a component of $\dot{\Omega}$ which is perpendicular to $\tilde{\Omega}_1$ but lies in the plane defined by $\tilde{\Omega}_1$ and $\tilde{\Omega}_2$. This radius cannot be obtained from the second-order PMD vector $\dot{\Omega}$.

While definition (21) is perfectly legal it has a weak point: Assume a link in which only first and (nonzero) second-order PMD defined by (21) are present. For high frequency offsets ω the length of the PMD vector, and hence the first-order DGD at frequency $\omega_0 + \omega$, become infinity. This is not easily understandable because first-order DGD is believed to have a Maxwell distribution with similar or equal expectation value for all frequencies. This argument also applies for $\geq$third-order PMD.

In this respect the model of two DGD sections is advantageous. It neglects the component of $\dot{\Omega}$ in direction of Ω that is small in ≤ 2 section models but gives the gyration radius, and a total DGD which does not approach infinity for large ω! The transmission span will most likely behave like concatenated fixed DGD sections according to the probabilistic arguments at the end of Section II-A. It is therefore more important to take care of this gyration by a two-section equalizer than to try to compensate even for that component of $\dot{\Omega}$ which has the direction of Ω.

As another example the transfer function of three DGD sections is given in (22) at the bottom of the page.

C. Number and Size of Differential Group Delay Sections

The simplest PMD equalizer is just a polarization transformer (SBA) placed at the transmitter side which adjusts the input polarization to be a PSP of the transmission span [3]. If the transmission span exhibits purely first-order PMD there is no residual penalty.

However, there is a correlation between first- and second-order PMD [defined by (21)] [13]. As an example the TS is assumed to consist of two sections with a DGD of $T/\sqrt{2}$ each, where T is the bit duration. The SBA in between them has a retardation of $\pi/2$, which is the statistical expectation value. The combined first-order DGD is T, a typical value for 10 Gb/s transmission over old fibers (100 ps). A 1-section equalizer with DGD T removes first-order PMD. Equation (22) has been plotted for this case in Fig. 6. The different curves depend on the relation between the input polarization and the DGD sections. A typical (optical) eye opening penalty $10 \log |H(\pi/T)|$ estimated from (16) at the Nyquist frequency is 2.5 dB. For comparison accurate eye simulations were also performed (insets), and the corresponding penalty was 2.2 dB for two out of three input polarizations, with marginal differences possible depending on chosen filtering. Apparently the small-signal transfer function is a good approximation of a complete numerical simulation. If the DGD's are divided by $\sqrt{2}$ the penalty drops to 0.7 dB, but the eye is completely closed if the DGD's are multiplied by $\sqrt{2}$.

A penalty of 2.2 dB may seem tolerable in some cases but it should be considered that PMD is not the only source of signal degradation. In WDM systems some residual uncompensated chromatic dispersion is normally present at least on the outer channels. Self- and cross-phase modulation, and crosstalk due to four-wave mixing or simply an imperfect WDM DEMUX circuit can also diminish the available eye opening. Finally the bandwidth limitation of transmitter and receiver also causes a
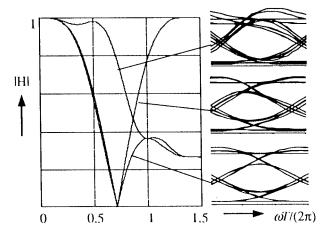

Fig. 6. Small-signal baseband transfer functions and eye diagrams for typical cases in which first-order PMD is compensated.

small eye closure. With all these effects considered additional penalties due to imperfect PMD compensation should be kept at a minimum. We conclude that *PMD should preferably be compensated also to higher order.* Another reason to use multisection compensators is that the acceptance of PMD equalization at the transmitter side by input polarization control ($\rightarrow$ backchannel, large propagation delay) or of a 1-section equalizer at the receiver ($\rightarrow$ variable DGD section needed) suffers also from a slow response for the reasons given in parentheses.

Since we have argued that variable DGD sections cannot be tolerated in multisection PMD equalizers we need to assess penalties caused by constant DGD's. A practical EQ with fixed DGD sections built according to the guidelines of Section II-A is not perfect in general, as may be seen from the example illustrated in Fig. 7. The DGD profiles of transmission span and equalizer were chosen identical. Two adjacent DGD sections of the TS initially compensate each other, just like two other DGD sections of the EQ. If these two TS DGD sections "unfold," i.e., if the SBA in between them changes its retardation from (to a lower value or zero, the differently located idle two EQ DGD sections must do the same thing until a new equilibrium of perfect PMD compensation is reached. This process was simulated, and the intermediate eye opening penalty was calculated (Fig. 8). The DGD of each of $N = 4$, 8, 16, 32 sections was chosen as $\tau = 0.4$, 0.28, 0.2, 0.14 $\cdot T$, respectively. Fortunately the penalties are not large. For example, 32 DGD sections with $0.14\,T$ each ($4.5\,T$ in total) have so far yielded ≤ 0.05 dB penalty. The penalty corresponds to a barrier between a side maximum and a main maximum

$$H(\omega) = \begin{pmatrix} \cos(\omega\tau_1/2)\cos(\omega\tau_2/2)\cos(\omega\tau_3/2) \\ -\sin(\omega\tau_1/2)\sin(\omega\tau_2/2)\cos(\omega\tau_3/2)\tilde{\Omega}_{1n}^T\tilde{\Omega}_{2n} \\ -\sin(\omega\tau_1/2)\cos(\omega\tau_2/2)\sin(\omega\tau_3/2)\tilde{\Omega}_{1n}^T\tilde{\Omega}_{3n} \\ -\cos(\omega\tau_1/2)\sin(\omega\tau_2/2)\cos(\omega\tau_3/2)\tilde{\Omega}_{2n}^T\tilde{\Omega}_{3n} \end{pmatrix} + j\sin(\omega\tau_1/2)$$
$$\cdot \begin{pmatrix} (\cos(\omega\tau_2/2)\cos(\omega\tau_3/2) - \sin(\omega\tau_2/2)\sin(\omega\tau_3/2)\tilde{\Omega}_{2n}^T\tilde{\Omega}_{3n})\tilde{\Omega}_{1n}^T \\ +(\cos(\omega\tau_1/2)\cos(\omega\tau_3/2) + \sin(\omega\tau_1/2)\sin(\omega\tau_3/2)\tilde{\Omega}_{1n}^T\tilde{\Omega}_{3n})\tilde{\Omega}_{2n}^T \\ +(\cos(\omega\tau_1/2)\cos(\omega\tau_2/2) - \sin(\omega\tau_1/2)\sin(\omega\tau_2/2)\tilde{\Omega}_{1n}^T\tilde{\Omega}_{2n})\tilde{\Omega}_{3n}^T \end{pmatrix} S_{\text{in}}. \tag{22}$$
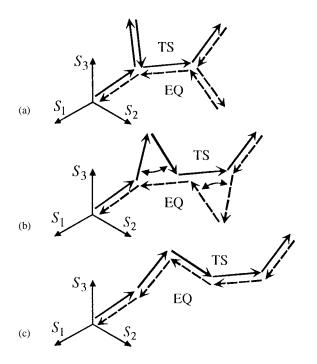
Fig. 7. (a) and (c) Transition between two perfect PMD compensation scenarios causes (b) imperfect PMD compensation.

during the control process. If the barrier is low enough it may be surmounted by noise ("annealing"). In this numerical example it is sufficiently low, and it becomes clear that fixed DGD sections need not be inferior in this respect to variable DGD sections.

Another issue is how well natural PMD can be compensated. In this context we can argue that full SBA's (retardation $0 \leq \varphi \leq \pi$) are not strictly needed: The SBA retardation needs to be near (only if the PMD vectors of two DGD sections of the TS join under this angle. However, if they do the enclosed area is small and not much performance will be lost if the PMD equalizer neglects to follow these two vectors forth and back and rather takes a shortcut in the PMD profile from the beginning of the first to the end of the second. A reasonable SBA retardation range may be $0 \leq \varphi \leq \pi/2$ (half mode conversion, "half SBA"), and this range is met or exceeded by the units of the distributed fiber-based PMD equalizer which is discussed later. In the following simulation the EQ therefore had $2N$ DGD sections of DGD $\tau/2$ each, separated by half SBA's (while N sections of DGD τ and full SBA's served as a performance reference). In each case the transmission span had $4N$ sections with DGD $\tau/\sqrt{8}$, and some correlation between the PSP's of neighboring sections was assumed. Although we think the data base is not yet satisfactory we give some preliminary results in Fig. 9. Since the (approximately) expected Maxwell distribution has a long tail not the maximum penalty but the average of the top 25% observed penalties is given at the right side, whereas the left side gives the average penalty. As an example, an equalizer with $2N = 64$ sections with DGD $\tau = 0.07T$ ($4.5T$ in total) has so far yielded ≤ 0.4 dB penalty.

It is also interesting to know whether the reference configuration (N, τ, full SBA's) performs better or, as expected, worse. In our simulations there is a trend in favor of the more distributed equalizer ($2N, \tau/2$, half SBA's).

Note that in Figs. 8 and 9 the contour lines of constant penalty are approximately parallel to the straight lines defined by $\sqrt{N}\tau$.

D. Penalty Signals

The ultimate goal of a PMD equalizer is to minimize the bit error ratio (BER). This quantity is neither available, nor can it be measured with high accuracy in a very short time. Also, the vectors $\boldsymbol{u}, \boldsymbol{v}, \boldsymbol{w}$ of Section II-B cannot be measured during normal operation. A useful means to detect PMD-induced penalties is spectral filtering in the electrical part of the receiver [4], [6], [14] because PMD affects the high-frequency parts of the signal spectrum first. If both PSP's of a medium with first-order DGD τ are equally excited a narrowband filter with center frequency f_c will yield a normalized output power $\cos^2(\pi f_c \tau)$. This function is ambiguous if τ can exceed $1/(2f_c)$. A system based on such a filter may lock into a false maximum which is purely generated by suboptimum signal analysis. However, PMD penalty detection can always be made unambiguous with moderate electronic effort. One possibility is to use several bandpass filters with center frequencies equal to 1, 1/2, 1/4, ... times the clock frequency $1/T$.

In a small spectral region the data signal spectrum can be understood to be white. A narrowband approximation allows its representation by Gaussian in-phase and quadrature components. The power at the filter output has a χ^2-distribution with two degrees-of-freedom. The quotient of squared mean to variance, i.e., the SNR, assumes the value to be one. Consider the impulse response of the narrowband filter to have the length T_1. We integrate the filter output (in theory: sum up the samples arriving every T_1) over a given measurement time T_2. The low-pass filtered signal then has a SNR $= T_2/T_1$ and is a χ^2-distribution with $2T_2/T_1$ degrees-of-freedom. Thermal noise plays a subordinate role in this context because it is a small constant fraction of the data signal. From the SNR viewpoint we see it is desirable to have as high as possible a filter bandwidth. On the other hand a high filter bandwidth fills the nulls of the $\cos^2(\pi f_c \tau)$ function, and a compromise has to be adopted therefore. At 10 Gb/s a practical SNR minimum of 40 dB may be obtained for $T_1 = 1$ ns, $T_2 = 10$ μs. The expected normalized output powers as a function of applied first-order DGD, normalized with respect to bit duration T, are plotted for several filters in Fig. 10. For small τ a wide highpass filter with a passband from $0.4/T$ to $1/T$ gives essentially the same response as a bandpass filter centered at $0.5/T$.

For simplicity ignore the highpass filter in the following discussion. While the lowest-frequency filter is in principle sufficient for PMD penalty measurement the highest frequency filter ($0.5/T$ or highpass filter) is definitely needed because it yields the sharpest response for small DGD's. In the experiments (Section IV) we have therefore adopted the
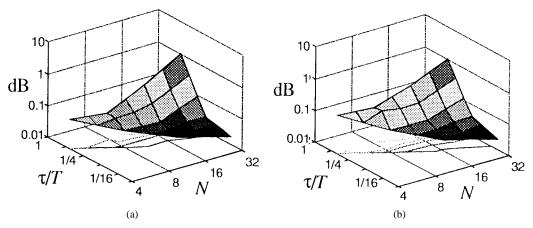
Fig. 8.   (a) Average and (b) maximum of maximum penalties observed during DGD section unfolding (Fig. 7). TS and EQ both have N sections of DGD τ each.
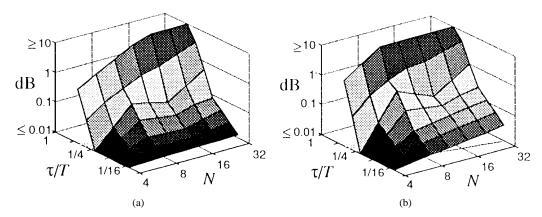

Fig. 9.   (a) Average and (b) maximum of top 25% penalties calculated for multisection PMD compensator. See text.

following strategy: if the lowest-frequency filter output signal ($0.125/T$ GHz) is below a threshold (e.g., 70%) it is used alone as a quality criterion to be maximized. Once it passes the threshold the next higher filter output signal ($0.25/T$) could be used in principle, and so on. Experimentally it turned out that maximization of the highest-frequency filter output signal alone ($0.5/T$ GHz) did not correspond to best BER, maybe due to nonlinear behavior of some system components. Therefore filter output signals ($0.5/T$ or $0.25/T$) were linearly combined with small portions of those of the lower-frequency filters ($0.25/T$ and $0.125/T$, or $0.125/T$) to a quality criterion if the latter signals all passed a threshold. Compared to the strategy with a fixed linear combination [6] our algorithm gives superior detection sensitivity for low DGD's while maintaining monotonicity for high DGD's, and allows to adjust for optimum BER performance.

We have verified that PMD equalization of RZ signals is also possible with the same strategy. Particularly good compensation can be obtained if the highest frequency bandpass filter selects the strong clock frequency line.

III. IMPLEMENTATION OF OPTICAL EQUALIZERS

Three optical equalizers will be presented which we have realized or considered. While this collection is by no means complete alternative implementations will also be discussed at the appropriate places.

A. Endlessly Rotatable Waveplates

Substantial work has been performed on optically broadband endless polarization control systems [15], [16], [8], and all these could be used in PMD compensators. Some of them apply occasional resets which does not preclude application in an equalizer because the above-derived requirement on polarization transformers is quite general. However, resets slow down operation, and we prefer to avoid resets by concentrating on polarization transformers with endlessly variable eigenmodes: Endless Soleil–Babinet compensators in LiNbO$_3$ have been operated successfully [15], [16], and a quarter-, half-, quarterwave plate configuration in LiNbO$_3$ was operated as an endless elliptical retarder at very high speed [8] and in a PMD compensator with a mechanical delay line [6].

Concerning nomenclature, note that we used to understand a "reset" to be any abrupt change of control parameters necessary to respond to an infinitesimal polarization change [15] while other authors seem to have redefined the word less conservatively. Consider the following example labeled reset-free: The polarization fed into a quarter-, half-, quarterwave plate arrangement is first elliptical with azimuth angle α, then becomes circular, then elliptical with azimuth angle $\alpha + 45°$, while the desired output polarization is always circular. Just when passing circular input polarization the first quarterwave plate has to flip by $45°$, and at least one of the other plates must also turn. This is a reset in the conservative sense.
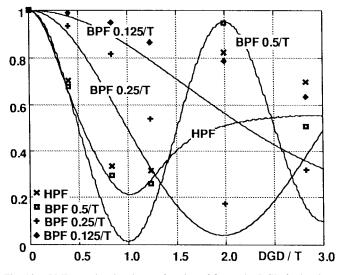
Fig. 10. PMD penalty signals as a function of first-order DGD for bandpass filters centered at $0.5/T$, $0.25/T$, $0.125/T$, and a high-pass filter with cutoff frequencies $0.4/T$ and $1/T$. Calculated values (lines) and measurement (symbols; see Section IV-A).

We now recall that the principal states of a polarization-maintaining fiber (PMF) are linear. In a PMD equalizer with DGD sections made of PMF the polarization transformers could, e.g., each consist of a quarter- and a halfwave plate because this configuration is able to endlessly transform any polarization into linear. In our present experiments we had no LiNbO$_3$ waveplates available. Fiberoptic waveplates, endlessly rotatable by stepper motors [17], were therefore realized. Since the standard fiber between the last waveplate and the splice to the next PMF may cause its PSP to appear elliptical we chose the quarter-, half-, quarterwave plate arrangement. As long as the PSP does not appear circular this application is reset-free even in the conservative sense because it has one more than the necessary number of degrees-of-freedom.

B. Ferroelectric Liquid Crystals

Liquid crystals are a class of nonmechanical polarization transformers. Nematic liquid crystals behave like waveplates of fixed orientations but variable retardations [18]. However, their speed is insufficient to follow manual fiber shaking. In contrast, ferroelectric liquid crystals (FLC's) work as waveplates of fairly constant retardations but can be rotated quite fast within limits [19]. A practical obstacle could be the relatively tight device tolerances needed to implement a reset algorithm like the one described in [14]. Here, we show that resets are not necessary.

Mode coupling adjustable in both quadratures [20] allows endless polarization control as long as the number of coupling sections is very large. However, *individual driving* allows to reduce the number of sections to just a few. A stack of FLC's with aligned axes can be considered to be a birefringent waveguide with mode coupling sections. The required minimum is three cells with retardations 1.895, 1.943, and 1.895 rad. The more cells there are, the lower are required tilt angles and fabrication accuracy. If available tilt angles are very small cell
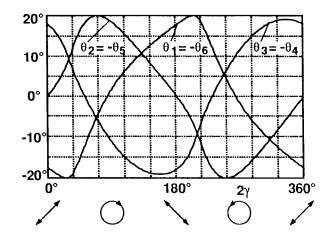

Fig. 11. Tilt angles for full mode conversion as a function of overall eigenmode.

retardations of $2\pi/3$ maximize the mode conversion that is available for the least favorably chosen coupling phase.

To give a realistic example, six FLC's with retardations 1.82, 2.57, 1.82, -1.82, -2.57, and -1.82 rad need tilt angles of $\pm 20°$, are controlled by just three different voltages (see Fig. 11), and tolerate retardation variations of $-36\% \ldots +12\%$. The negative retardations can be replaced by positive ones if the respective cells are turned by $90°$. This arrangement can convert x- into y-polarization by any set of tilt (= azimuth) angles $\vartheta_1 \ldots \vartheta_6$ given in Fig. 11 (which functions are, by the way, not the only possible solution). The overall retardation is π in this case. Jones and normalized Stokes eigenvectors are $[\exp(j\gamma) \ \exp(-j\gamma)]^T/\sqrt{2}$ and $[0 \ \cos 2\gamma \ \sin 2\gamma]^T$, respectively. The eigenvector locus is the $S_2 - S_3$ great circle of the Poincaré sphere and contains the sketched polarization ellipses. Arbitrary output polarization can be generated if all $\vartheta_1 \ldots \vartheta_6$ corresponding to a certain value $0° \leq 2\gamma < 360°$ are multiplied by a common factor between "0" and "1." In those cases the eigenmode locus is in general not the $S_2 - S_3$ great circle. The complete polarization transformer can be described as an SBA plus a PS with a retardation depending on the SBA parameters, see (11). Since only two degrees-of-freedom are needed the six tilt angles provide substantial redundancy.

Eigenmodes (indexes $\pm$) and retardation of a cell were determined as a function of applied voltage (Fig. 12). Physical azimuth angles $\vartheta_\pm$ changed by $35°$, and left- to right-elliptical behavior was observed with a $35°$ change of the ellipticity angles $\varepsilon_\pm = \pm\arctan(a/b)$ where a and b are the minor and major ellipse axes, respectively. Angles $2\vartheta, 2\varepsilon$ characterize the rotation axis position in polar coordinates on the Poincaré sphere. Measured elliptical birefringence is believed to be due to chiral molecule and helical supermolecular structure. While $\pm 17.5°$ azimuth angle change alone is not sufficient to implement the discussed polarization transformer with six FLC's, the simultaneous ellipticity change makes the eigenmodes sufficiently variable in total. The retardation was ~ 2.8 rad ($160°$). The DHF response time constant was determined as 200 μs. Recovery from saturation after application of too high voltages may need several ms but is not of importance in a well-designed system.
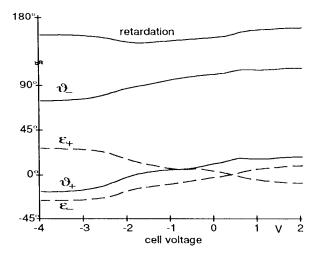
Fig. 12. Eigenmodes (azimuth angles $\vartheta_\pm$, ellipticity angles ε_{pm}) and retardation of deformed-helix ferroelectric liquid crystal cell.

Fig. 13. Distributed PMD equalizer with PMF twisters.

Fig. 14. Twist angles required to transform x-polarization at the input into a desired output polarization (half-mode conversion with arbitrary phase angle).

C. Distributed Equalizer

The issue of cascading a large number of DGD sections in an equalizer seems to have been neglected in the published literature, probably due to the coupling losses between DGD sections and polarization transformers. We have therefore implemented DGD sections and polarization transformers in a single polarization-maintaining fiber (PMF).

The required endless transformations of any polarization into linear can be implemented by a finite number of PMF twist sections [21] for mode coupling. We describe one out of many possible implementations: Two variable twisting points, suitably placed between two fixed twisting points (Fig. 13, inset) are sufficient to transform x-polarization ($S_1 = 1$) into any polarization with equal power splitting between x and y (Fig. 14). Twisted fiber lengths are 0.21, 0.38, 0.21 times the beat length Λ. The abscissa scaling in Fig. 14 is this time not an eigenmode but refers to the output polarization $[\exp(-j\gamma) \; \exp(j\gamma)]^T/\sqrt{2}$ for x-polarized input. Smaller angles α_1, α_2 allow to generate any linear or elliptical polarization with dominating x-polarization ($S_1 > 0$). Two half mode converters can be combined for full mode conversion. In other words, two subsequent pairs of fiber twisters can be operated as one endless polarization transformer equal to an SBA plus a PS that partly depends on the SBA parameters. The PMF length in between the two twister pairs determines of
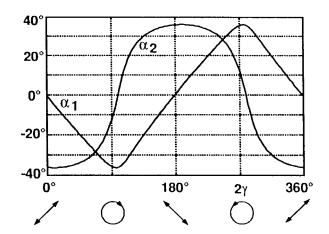
course the optical bandwidth and the necessary phase relations between applied twist functions.

The beat length of a commercially available, weakly polarization-maintaining fiber was determined to be $\Lambda = 21.6$ mm @ 1550 nm, which corresponds to a DGD of 0.24 ps/m. A 322-m long PMF piece was pulled through the hollow axes of 64 stepper motors. The fiber was fixed inside and outside the axes to define twist sections. For easier mounting the variable twist points had lengths Λ rather than zero. PMF lengths were 2 m between the first three motor pairs so that a possible failure of one of them would not matter, and then 11 m. A total DGD of 77 ps could thus be commanded, with available degrees-of-freedom corresponding to ~16 endless polarization transformers (full SBA's) and DGD sections. Total loss was 1.7 dB initially, mainly determined by one connector and two splices to standard fiber. Due to careless handling the PMF was broken later, and repaired by a bad splice which brought the total attenuation to 2.2 dB.

In a separate setup we were able to show ≥90% mode conversion when 2 × 2 adjacent stepper motors were operated with sinusoidal twist functions of different amplitudes and phases. In contrast, the truly required functions (Fig. 14 with the possibility of abscissa distortion) differ substantially from sinusoids. The large mode conversion result lets expect endless polarization control to be possible.

As a possible simplification it should be mentioned that exact twist lengths become unimportant if the number of twisters is approximately doubled, for the following reason: In each polarization transformer mode coupling should be possible both in phase and in quadrature. An arbitrarily placed fiber twist section will, with probabilities of one-half each, be closer to in-phase or to quadrature mode coupling. Compared to the case of known coupling phases more twisters will therefore be needed.

The fiber-optic implementation of a distributed PMD equalizer has the advantage of being tailorable to almost any DGD. However, the same principle could also be realized in X-cut, Y-propagation LiNbO$_3$, where DGD sections and polarization transformers would be integrated on one birefringent chip by simply cascading a number of mode converters [20]. Available total DGD is limited to ~0.26 ps/mm while chip lengths are
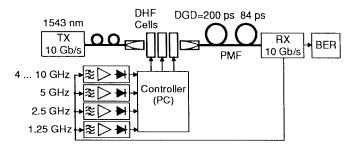
Fig. 15.   A 10-Gb/s transmission setup with three ferroelectric liquid crystals.

typically <100 mm. Compensation of DGD's larger than 26 ps therefore requires some cascading or beam folding.

IV. TRANSMISSION EXPERIMENTS

Transmission experiments have been conducted with each of the three mentioned PMD equalizers or polarization transformers. The bit rate is not believed to be critical for the PMD compensation process if DGD is scaled with bit duration. The experimental bit rate was in each case determined by available hardware.

A. 10 Gb/s with Input Polarization Control

A single polarization transformer (SBA) may be placed at the transmission span input in order to avoid first-order PMD by selecting a PSP [3]. Three ferroelectric liquid crystals were used for this purpose in a 10 Gb/s system. According to the discussion in Section III-B, the setup (Fig. 15) did not permit endless polarization control.

Different lenghts of PMF with some manual polarization controllers simulated 40, 84, 200, or 284 ps DGD of the transmission span.

In the electrical part of the receiver a four-channel PMD penalty detector was implemented, consisting of 1.25, 2.5, and 5 GHz bandpass filters (with bandwidths 0.9, 0.5, and 0.6 GHz, respectively) and a 4-...10-GHz high-pass filter. Buffer amplifiers with subsequent power detectors provided DC output signals. The simulated behavior of these PMD penalty signals has already been shown in Fig. 10, but experimental data points are also plotted therein for comparison. The measured signal extrema are less accentuated than predicted. We believe this is mainly due to rough filter transfer functions since no care was taken to get them smooth.

The quality criterion was generated as explained in Section II-C. It was also experimentally verified that the highpass filter can replace the 5-GHz bandpass filter.

The back-to-back eye diagram is shown in Fig. 16(a). With DHF cells and PMF's with a total DGD of 284 ps a very similar eye diagram [Fig. 16(b)] was obtained when the controller was switched on. A gradient (peak search) algorithm was used to optimize the eye diagram opening as estimated by the penalty signals. Other configurations are shown for 84 and 200 ps of DGD, and similar results were obtained for 40 ps. The controller was either set up for signal maximization ["best case," Figs. 16(c), (e) or minimization ["worst case," Figs. 16(d), (f); for test purposes]. In the "best cases" the
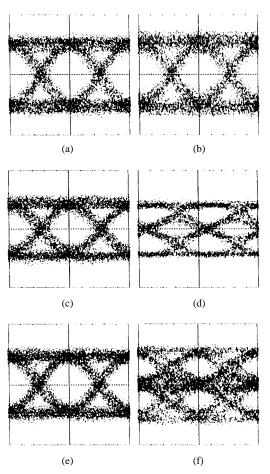

Fig. 16.   10 Gb/s eye diagrams. (a) back-to-back, (b) 284 ps, best case, (c) 84 ps, best case, (d) 84 ps, worst case, (e) 200 ps, best case, and (f) 200 ps, worst case.

measured BER was less than 10^9. For example, with 284 ps of DGD the system was operated error-free for half an hour.

B. 40 Gb/s with Three-Section Equalizer

A PMD equalizer for the receiver of a 40-Gb/s transmission system was setup, consisting of three PMF sections with 10 ps DGD each, and three groups of fiberoptic $\lambda/4, \lambda/2, \lambda/4$ plates, endlessly rotatable by stepper motors [22] (Fig. 17).

Further details of the transmission system have been described in [23]. Two polarization-maintaining fiber (PMF) pieces of 20 and 10 ps DGD, respectively, and manual polarization transformers simulated the PMD of a fiber link. PMD penalty extraction was performed at 20, 10, and 5 GHz. A PC worked as a controller and generated the stepper motor driving signals.

Without any PMF a good eye diagram was achieved [Fig. 18(a)]. With PMD simulator and unadjusted PMD compensator in place the eye was closed [Fig. 18(b)]. However, with automatic control an open eye was readily obtained [Fig. 18(c)]. A gradient (peak search) algorithm maximized a linear combination of the three penalty signals.

If any one of the three control signals was used alone compensation failed repeatedly, and the eye diagram remained closed. This can be understood from the fact that the total added DGD of PMD simulator and compensator was 60 ps,
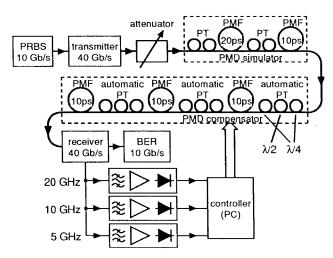
Fig. 17. A 40-Gb/s transmission system with fiber-optic three-section PMD equalizer.
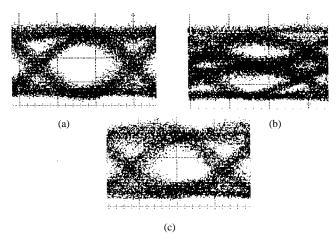

Fig. 18. (a) The 40 Gb/s eye diagrams: back-to-back; (b) with PMD simulator and unadjusted compensator; (c) with PMD simulator and working PMD compensator.
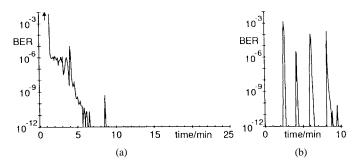

Fig. 19. (a) BER records of one out of four 10 Gb/s data streams as a function of time: initial PMD compensation convergence; (b) responses to four manual changes of fiber loop settings.
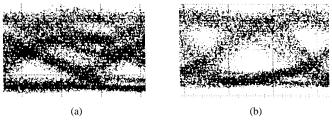

Fig. 20. (a) 40 Gb/s eye diagrams: with PMD simulator; (b) with PMD simulator and working input polarization control.
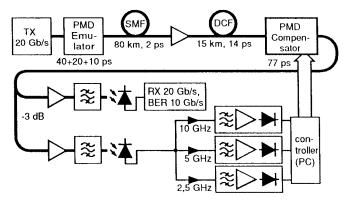

Fig. 21. 20 Gb/s transmission setup with distributed fiber-based PMD compensator.

more than $2T$. On the other hand, the combination of 5- and 10-GHz BPF signals was sufficient to attain a relative optimum, but it was degraded with respect to the case of all three signals being available.

The BER was recorded as a function of time. After initial convergence nearly error-free operation was observed [Fig. 19(a)]. The ability of the system to recover from disturbances was assessed separately. Manual changes of fiber loop settings caused a momentarily high BER but were quickly compensated thereafter [Fig. 19(b)].

Input polarization control was also tried. To do so, the PMD simulator was removed, and the first polarization transformator of the compensator was used for control. The rest of the compensator, 3×10 ps of DGD and two formerly automatic polarization transformers, worked now as a PMD simulator. The initial eye pattern, completely closed, is seen in Fig. 20(a). With input polarization control good BER performance was again obtained. However, PMD was not fully removed which can be seen from a somewhat distorted eye diagram [Fig. 20(b)], as has been discussed in Section II.

The experiment shows that PMD compensation is possible at the highest bitrate that is presently used for electrical TDM transmission systems. In contrast to electronic PMD compensation [7] the optical scheme allows to compensate for larger DGD's, does not increase the noise bandwidth of the receiver, and does not impair the eye diagram like any added electronic circuit would at these high frequencies.

C. 20 Gb/s with Distributed Fiber Optic Equalizer

Best performance was expected from the distributed fiberoptic equalizer. A 20-Gb/s transmission system [24] was used to test the compensator (Fig. 21). The data signal was transmitted through a PMD emulator, 80 km of standard fiber (SMF) with a DGD of 2 ps, and 15 km of chromatic dispersion compensating fiber (DCF) with a DGD of 14 ps [25]. The emulator was the compensator of the 40-Gb/s experiment but section DGD's were 40-, 20-, and 10-ps DGD this time. PMD penalty detection occurred at 10, 5, and 2.5 GHz. For
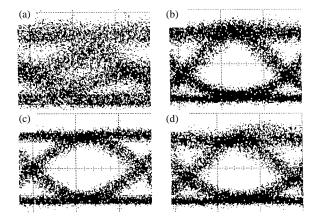
Fig. 22. 20 Gb/s eye diagrams: (a) PMD distortion; (b) compensator alone; (c) back-to-back; (d) with emulator $(40 + 20 + 10$ ps), SMF (2 ps), DCF (14 ps), and compensator (77 ps).
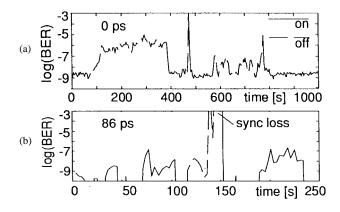

Fig. 23. BER records of one out of two 10 Gb/s data streams as a function of time with compensator ON/OFF for different DGD values of transmission span.

convenience the optical power was split to an extra photodiode. A gradient algorithm operated the 64 stepper motors. The response time of the whole compensator was ~1 s.

In all performed experiments the eye pattern was usually closed [example: Fig. 22(a)] unless the compensator was in operation. In a first test, the other fibers were left out, and the compensator was used alone [eye diagram: Fig. 22(b)]. The receiver sensitivity was −28 dBm which is comparable to back-to-back operation [Fig. 22(c)]. Measured BER was stable unless the compensator was turned off [Fig. 23(a)]. Then the PMD emulator with eight motorized fiber coils rotating at different speeds and the fibers were inserted. The resulting endless PMD variations with up to 86 ps of total DGD were very well compensated [Fig. 22(d)]. When the equalizer was stopped the BER increased drastically, but it dropped down when control was turned on again [Fig. 23(b)]. With increased power (−25 dBm) operation was error-free.

As expected the eye diagrams obtained with the distributed compensator looked nicer than those of the experiment with the three-section equalizer, not only due to the higher bit rate in the latter. The fact that total DGD's of 0 or up to 86 ps could be tolerated fully validates the principle of a compensator with fixed DGD sections. Indeed, the compensator also worked well in other situations, e.g., with $10 + 10$ ps of DGD to

be compensated. It worked even when these additional pieces of PMF were added to the normal setup (106 ps of DGD to be compensated in the worst case) but only when the fiber coils were not rotated.

Note that the eye diagrams with working compensator were somewhat peaked, especially if the compensator had nothing to do [Fig. 22(b)]. The effect was also more pronounced than in Fig. 18(c) where it can also be seen. Peaked eye diagrams occur in RZ systems and generally improve sensitivity. We believe the equalizer used its free capacity for eye opening maximization by introducing some beneficial higher order PMD.

V. DISCUSSION

In this section, we compare the relative merits of the different components and systems described in the preceding subsections.

1) Sections III-B and IV-A: Ferroelectric liquid crystals need fiber-to-fiber coupling. The best place for them is where this causes least extra expense, and this is in the collimated beam behind the isolator of a transmitter laser or at the output of an EDFA at the receive end. The 10-Gb/s experiment validates the general usefulness of these devices for selecting a PSP at the transmitter but still lacks the theoretically explained endlessness of the control scheme. Temperature stability and reliability research on these components is needed as well as a good packaging technology. It is therefore believed that these elements will not be the first to be used in commercial PMD compensators.

2) Sections III-A and IV-B: Soleil–Babinet compensators and rotatable waveplates are workhorses of polarization control since decades. Here the latter have been used in a PMD equalizer with three sections and, with less success as expected, for selecting a PSP at the transmitter side. While the 40 Gb/s experiment features the highest bit rate for which PMD compensation has been reported the mechanical waveplates are too slow for practical application. However, X-cut, Z-propagation LiNbO$_3$ allows to integrate Soleil-Babinet compensators or waveplates. Response times are short, and a few polarization transformers and DGD sections will provide satisfactory compensation in all cases where DGD range requirements are not very demanding.

3) Sections III-C and IV-C: By far the best performance is obtained with multisection or distributed PMD equalizers, including cases where a first-order PMD compensator with variable DGD will be insufficient. In the 20-Gb/s experiment, a compensated-DGD-times-bitrate-product of 1.7 has been demonstrated with an equalizer having about 16 endless polarization transformers. Both these values are the highest reported to date. Especially here, but also at 40 Gb/s with only three DGD sections, beneficial eye diagram peaking has been observed. The fiber-based distributed compensator features lowest loss and a speed sufficient for those cases where the fiber is not moved. However, more compact and much faster PMD equalizers can be expected from an alternative implementation of this device in X-cut, Y-propagation LiNbO$_3$. For high-end PMD compensation at 10 Gb/s, and for any PMD compensation at 40 Gb/s, this is the preferred solution.

VI. Summary

PMD, especially in "old" fibers, impairs system performance of high-capacity trunk lines. As we have shown, a suitable optical PMD equalizer should have several or many differential group delay (DGD) sections with polarization transformers in between, which can endlessly transform any input polarization into a principal state of the following DGD section. The sections must practically have fixed DGD's unless there is only one section. The small-signal baseband transfer function for PMD has been introduced and evaluated, and the necessary number of DGD sections has been discussed.

A PMD equalizer with PMF pieces and endlessly rotatable fiber coils has been realized. For increased speed an endless polarization transformer with ferroelectric liquid crystal cells has been proposed for PMD compensation, but the present experimental setup does not yet provide endless operation. Optimum performance is obtained with a distributed PMD equalizer because it can compensate also higher order PMD. A fiber-based equalizer with 64 stepper motors has been implemented. Its principle can also be realized in $LiNbO_3$. Finally, transmission experiments at 10, 20, and 40 Gb/s with these PMD equalizers and a purely electrical PMD detection scheme have proven the validity of the presented concepts. Stable operation with well-opened eye diagrams has been obtained. The distributed equalizer has allowed excellent compensation of up to 1.7 bit durations of total DGD. A pure first-order PMD compensator would have been insufficient in this situation due to higher order PMD.

References

[1] C. D. Poole and R. E. Wagner, "Phenomenological approach to polarization dispersion in long single-mode fibers," *Electron. Lett.*, vol. 22, no. 19, pp. 1029–1030, 1986.
[2] J. Peters, A. Dori, and F. Kapron, "Bellcore's fiber measurement audit of existing cable plant for use with high bandwidth systems," in *Proc. NFOEC'97*, San Diego, CA, Sept. 21–25, 1997, vol. 2, pp. 19–30.
[3] T. Ono, S. Yamazaki, H. Shimizu, and K. Emura, "Polarization control method for suppressing polarization mode dispersion influence in optical transmission systems," *J. Lightwave Technol.*, vol. 12, pp. 891–898, May 1994.
[4] T. Takahashi, T. Imai, and M. Aiki, "Automatic compensation technique for timewise fluctuating polarization mode dispersion in in-line amplifier systems," *Electron. Lett.*, vol. 30, no. 4, pp. 348–349, 1994.
[5] M. Yoshimura, T. Kudo, and T. Ozeki, "Polarization mode dispersion equalization," in *Proc. OEC '94*, Makuhari Messe, Japan, 1994, vol. 14E-12, pp. 258–259.
[6] F. Heismann, D. A. Fishman, and D. L. Wilson, "Automatic compensation of first-order polarization mode dispersion in a 10-Gb/s transmission system," in *Proc. ECOC '98*, Madrid, Spain, vol. WdC11, pp. 529–530.
[7] D. Schlump, B. Wedding, and H. Bülow, "Electronic equalization of PMD and chromatic dispersion induced distorsion after 100 km standard fiber at 10 Gbit/s," in *Proc. ECOC '98*, Madrid, Spain, vol. WdC14.
[8] F. Heismann and M. S. Whalen, "Broadband reset-free automatic polarization controller," *Electron. Lett.*, vol. 27, no. 4, pp. 377–379, 1991.
[9] M. Johnson, "In-line fiber-optical polarization transformer," *Appl. Opt.*, vol. 18, no. 9, pp. 1288–1289, 1979.

[10] F. Curti *et al.*, "Statistical treatment of the evolution of the principal states of polarization in single-mode fibers," *J. Lightwave Technol.*, vol. 8, pp. 1162–1166, Aug. 1990.
[11] F. Matera, "Evolution of polarization mode dispersion in single mode fibers," in *Proc. EFOC/LAN '92*, Paris, France, 1992, pp. 16–21.
[12] G. J. Foschini and C. D. Poole, "Statistical theory of polarization dispersion in single-mode fibers," *J. Lightwave Technol.*, vol. 9, pp. 1439–1456, 1991.
[13] H. Bülow, "System outage probability due to first- and second-order PMD," *IEEE Photon. Technol. Lett.*, vol. 10, pp. 696–698, 1998.
[14] D. Sandel, S. Hinz, M. Yoshida-Dierolf, J. Gräser, R. Noé, L. Beresnev, T. Weyrauch, and W. Haase, "10-Gb/s PMD compensation using deformed-helical ferroelectric liquid crystals," in *Proc. ECOC '98*, Madrid, Spain, vol. WdC24, pp. 555–556.
[15] R. Noé, H. Heidrich, and D. Hoffmann, "Endless polarization control systems for coherent optics," *J. Lightwave Technol.*, vol. 6, pp. 1199–1207, July 1988.
[16] N. G. Walker and G. R. Walker, "Polarization control for coherent optical communications," *J. Lightwave Technol.*, vol. 8, pp. 438–458, Mar. 1990.
[17] T. Matsumoto and H. Kano, "Endlessly rotatable fractional-wave devices for single-mode-fiber optics," *Electron. Lett.*, vol. 22, pp. 78–79, 1986.
[18] S. R. Asham, M. C. K. Wiltshire, S. J. Marsh, and A. J. Gibbons, "A practical liquid crystal polarization controller," in *Proc. ECOC'90*, Amsterdam, The Netherlands, vol. 1, pp. 393–396.
[19] L. A. Beresnew, V. G. Chigrinov, D. I. Dergachev, E. P. Pozhidaev, J. Fünfschilling, and M. A. Schadt, "Deformed helix ferroelectric liquid crystal display: A new electrooptic mode in ferroelectric chiral smectic C liquid crystals," *Liquid Crystals*, vol. 5, p. 1171, 1989.
[20] F. Heismann and R. Ulrich, "Integrated-optical single-sideband modulator and phase shifter," *IEEE J. Quantum Electron.*, vol. 18, pp. 767–771, Apr. 1982.
[21] R. Ulrich and A. Simon, "Polarization optics of twisted single mode fibers," *Appl. Opt.*, vol. 18, pp. 2241–2251, 1979.
[22] D. Sandel, M. Yoshida-Dierolf, R. Noé, A. Schöpflin, E. Gottwald, and G. Fischer, "Automatic polarization mode dispersion compensation in 40 Gbit/s optical transmission system," *Electronics Letters*, vol. 34, no. 23, pp. 2258–2259, 1998.
[23] W. Bogner, E. Gottwald, A. Schoepflin, and C.-J. Weiske, "40 Gbit/s unrepeatered optical transmission over 148 km by electrical time division multiplexing and demultiplexing," *Electron. Lett.*, vol. 33, pp. 2136–2137, 1997.
[24] W. Bogner *et al.*, "20 Gbit/s TDM nonrepeatered transmission over 198 km DSF using Si-bipolar IC for demultiplexing and clock recovery," in *Proc. ECOC '96*, Oslo, Norway, vol. 2, pp. 203–206.
[25] R. Noé, D. Sandel, M. Yoshida-Dierolf, S. Hinz, C. Glingener, C. Scheerer, A. Schöpflin, and G. Fischer, "Fiber-based distributed polarization mode dispersion compensation at 20 Gb/s," *Electron. Lett.*, vol. 34, no. 25, pp. 2421–2422, 1998.

Reinhold Noé was born in Darmstadt, Germany, in 1960. He received the Dipl.-Ing. and Dr.-Ing. degrees in electrical engineering from the Technical University of Munich, Germany, in 1984 and 1987, respectively. His doctoral thesis was on endless polarization control.

He spent one Postdoctoral year at Bellcore, Red Bank, NJ. In 1988, he joined the Siemens Research Laboratories, Munich, working on coherent optical systems. Since 1992, he has been the Chair of Optical Communications and High-Frequency Engineering in the Department of Electrical Engineering at the University of Paderborn, Germany. In the area of optical communications, he is working on PMD compensation, applications of lithium niobate devices, and fiber Bragg gratings.

David Sandel was born in Wangen/Allgäu, Germany, on December 26, 1966. He received the Dipl.-Ing. degree in electrical engineering from the Technische Hochschule Karlsruhe, Germany, in 1992 and the Dr.-Ing. degree in fiber Bragg gratings.

In 1992, he joined the Chair of Optical Communications and High-Frequency Engineering in the Department of Electrical Engineering at the University of Paderborn, Germany. His current research interests concentrate on PMD compensation.

M. Yoshida-Dierolf, photograph and biography not available at the time of publication.

Stephan Hinz was born in Holzminden, Germany, on October 25, 1966. From 1988 to 1993, he studied electrical engineering at the University of Paderborn, Germany.

After receiving the Dipl.-Ing. degree, he joined the Chair of Optical Communications and High-Frequency Engineering in the Department of Electrical Engineering at the University of Paderborn, Germany. He works in the area of multigigabit optical transmission systems. His current research concentrates on penalty signal generation for PMD compensation.

V. Mirvoda, photograph and biography not available at the time of publication.

A. Schöpflin, photograph and biography not available at the time of publication.

C. Glingener, photograph and biography not available at the time of publication.

E. Gottwald, photograph and biography not available at the time of publication.

C. Scheerer, photograph and biography not available at the time of publication.

G. Fischer, photograph and biography not available at the time of publication.

Thomas Weyrauch was born in Erbach, Germany, in 1962. He received the diploma degree in physics from the Darmstadt University of Technology, Germany, in 1990 and the Dr. degree in 1997.

Since 1991, he has been working in the Institute of Physical Chemistry of the Darmstadt University of Technology. His research interests are focused on electrical and optical properties of liquid crystals and polymers and their applications.

Wolfgang Haase was born in Reinholdshain/Saxonia, Germany, in 1936. He received the Eng.-Dipl. degree in chemical engineering from the University of Magdeburg, Germany, in 1957 and the Diploma and Dr. degrees in chemistry from the University of Jena, Germany, in 1960 and 1964.

After Postdoctoral studies at Stockholm, Göteborg, and Uppsala, Sweden, and Marburg, Germany, he habilitated in structural and physical chemistry at the University of Marburg, Germany, in 1970. Since 1971, he has been Professor of Physical Chemistry at the Darmstadt University of Technology, Germany. His research interests are mainly devoted to properties and applications of liquid crystals, as well as nonlinear optics in polymers, magnetism of inorganic compounds, and bioinorganic chemistry.